Anomalous stress diffusion in earthquake triggering: Correlation length, time dependence, and directionality

Anomalous stress diffusion in earthquake triggering: Correlation length, time dependence, and directionality

Mireille Huc and Ian G. Main
School of GeoSciences, Edinburgh University, Edinburgh, UK

Received 14 November 2001; revised 23 October 2002; accepted 27 February 2003; published 1 July 2003.

[1] It has been recently suggested that moderate and large earthquakes can be triggered by similarly sized events at very long range. Here we study the main characteristics of earthquake triggering by determining its correlation length, time dependence, and directionality. The problem is examined at a global level, by using the Harvard centroid moment tensor catalogue. Our results show that the correlation lengths depend only weakly on the magnitude thresholds involved. No significant systematic triggering is observed for distances greater than the lithospheric thickness (100–150 km), and the correlation length magnitude is similar to the seismogenic thickness (10–20 km). The mean triggering distance and correlation length both increase with time very slowly compared with what would be expected from a normal diffusion process. This is consistent with a clock advance on the failure time based on the constitutive rules for subcritical crack growth following a transient change in the loading stress. The power law scaling disappears after a few months. A functional form for the probability of triggering as a function of time and distance is proposed on the basis of the properties of near critical point systems. The model fits the data well and could be used to calculate conditional probabilities for time-dependent seismic hazard due to earthquake triggering. An apparent directionality effect that was observed in the data set can be attributed to an artefact of poor depth determination. These results do not preclude individual long-range triggering with a potential directionality effect, but they do rule out a statistical correlation at distances much greater than the thickness of the lithosphere. *INDEX TERMS:* 7230 Seismology: Seismicity and seismotectonics; 7223 Seismology: Seismic hazard assessment and prediction; 8164 Tectonophysics: Stresses—crust and lithosphere; *KEYWORDS:* earthquake triggering, stress diffusion, criticality

Citation: Huc, M., and I. G. Main, Anomalous stress diffusion in earthquake triggering: Correlation length, time dependence, and directionality, *J. Geophys. Res.*, *108*(B7), 2324, doi:10.1029/2001JB001645, 2003.

1. Introduction

[2] When an earthquake occurs, the surrounding Earth volume is subject to a sudden change in dynamic stress associated with the passage of seismic waves and in static elastic stress, with a spatial distribution whose amplitude decays with distance. These stress changes may then induce further earthquakes, either in the form of smaller aftershocks in the immediate vicinity of the main shock (i.e., at a distance of around one source dimension), or in the form of long-range triggered events (several source dimensions). The evidence for longer-range triggering is not conclusive, although there are several case studies which suggest that very long-range triggering (at distances greater than a few hundred km) does occur in individual sequences. For example, the increase in seismicity in the western United States that followed the Landers, California, earthquake of 28 June 1992 is considered to be due to a triggering effect [*Hill et al.*, 1993]. Various physical explanations have been proposed for earthquake triggering [see *Harris*, 1998], the most compelling of which to date is the correlation with Coulomb stresses [*King et al.*, 1994; *Stein et al.*, 1994; *Harris et al.*, 1995; *Stein*, 1999]. However, these changes (in static or dynamic stress) seem too small on their own to explain long-range triggering like that observed after the Landers earthquake, which occurred at very large distances compared with the source dimension. As a consequence, it is necessary to invoke additional nonlinear amplification effects such as interactions between dynamic strains and crustal fluids, or to invoke a preexisting stress field which is already in a near-critical state. This explanation is consistent with the spatial correlation of the triggered seismicity following the Landers event with the locations of hydrothermal springs [*Hill et al.*, 1993]. However, long-range triggering is also seen in some instances where a nonlinear hydrothermal mechanism is not obvious. In this case the most likely explanation is an amplification effect based on

0148-0227/03/2001JB001645$09.00

rate and state dependent friction [see *Scholz*, 1998]. In this framework, earthquake triggering may occur due to a sudden change in the normal stress across faults [*Linker and Dieterich*, 1992], amplified by an effective rapid increase in strain rate, leading to a "clock advance" for earthquakes that may have been near failure prior to the main shock [*Gomberg et al.*, 1997]. The rate dependence in the underlying constitutive rules implies that the occurrence of long-range triggering should have some associated time dependence and provides a possible rationale for unifying the mechanism of short-range aftershocks with longer-range triggering.

[3] If the orientation of the fault plane of the triggering event and the local effective coefficient of static friction are known, and the presence of optimally oriented faults around the main shock is assumed, then calculations of the Coulomb stress changes induced by large events can be used to predict zones where aftershocks should preferentially occur [*King et al.*, 1994]. The same technique can also be used to model sequences of larger triggered events at longer range [*Stein et al.*, 1997]. At present, this technique cannot easily be performed on global data sets, because of the lack of global knowledge of the relevant model parameters, notably the inherent ambiguity of which nodal plane is the true fault plane in a focal mechanism. As a consequence, global studies are forced to focus more on a first-order, model-independent, statistical analysis of primary seismicity catalogues containing information on source magnitude and focal mechanisms, or preferably moment tensor catalogues. For example, *Gasperini and Mulargia* [1989] performed a statistical analysis of seismicity in Italy and found an "influence region" from 14 to 60 days after the event, at distances between 80 and 140 km. *Reasenberg* [1999], who studied foreshock occurrence (earthquakes with $m_b \geq 5.0$) before large earthquakes ($m_b \geq 6.0$ or $m_b \geq 7.0$) with worldwide catalogues, found no interaction at interevent distances greater than 75 km and interevent times greater than 10 days. *Lomnitz* [1996] studied the occurrence of only the largest earthquakes occurring this century ($m_b \geq 7.0$), and concluded that the very long range correlations observed after the Landers earthquake may be a general feature for such large events. Moreover, in the same study, an apparent gap in seismicity was observed at intermediate distances (around 300 km) for this set of data ($m_b \geq 7.0$). This apparent gap was attributed to a characteristic length effect, associated with a preferential directional distribution of triggered events (in the main shock dilatational quadrants). However, not all studies support the existence of a strong directional effect: for example, *Kagan and Jackson* [1998, p. 345] studied the spatial clustering of shallow aftershock hypocenters with respect to the focal mechanisms of main shocks and concluded that "normal stress has little or no influence on aftershock occurrence", implying a stronger strain rate control.

[4] Our approach uses a combination of some of the model-independent techniques described in the previous paragraph. The results can then be used as a suitable null hypothesis for future more detailed work on the global distribution of Coulomb stress triggering when the data become available. We first try to determine the region (both in time and space) over which correlations seem to exist in earthquake occurrence (the "influence region" defined by *Gasperini and Mulargia* [1989]) for worldwide data and various magnitude bands (from $M_w \geq 5.0$). We find that the spatial correlation can be fitted well by distributions predicted from percolation theory or near-critical point phenomena, for a finite correlation length. This allows us to examine the relationship between the observed correlation lengths and the magnitudes of the triggering and triggered events. The study of the evolution of the spatial correlation with respect to time should also give some insights into the physical mechanisms involved in earthquake triggering (in a broad sense, including both aftershock zones and regions of possible longer-range triggering). The knowledge of the focal mechanism of the triggering event allows us to determine the first-order features of directional effects from the orientation of the subsequent triggered events. The aim of the second part of our study is to determine if a systematic difference is observed between the dilatational and the compressional quadrants for the frequency of triggered events and hence to test the hypothesis that the normal stress change has a first order influence on the triggering probability. To perform the two parts of this analysis with the most homogeneous set of data possible, we use the centroid moment tensor (CMT) catalogue provided by Harvard University [*Dziewonski et al.*, 2001], which gives the focal mechanism for all the reported events from 1977.

[5] We first describe the principles of the analysis, and the necessary corrections that have to be taken into account to be able to interpret the results uniquely in terms of triggering. An important component of this is the spatial heterogeneity in the locations of seismic sources which is due to clustering of seismicity at plate boundaries. This effect has to be carefully removed to prevent spatial correlations being projected into temporal ones. We then present the results obtained by applying this analysis to the CMT catalogue in terms of evolution of the correlation with space and time and as a function of the threshold magnitude. After describing the method used to determine the quadrantal distribution of triggered events, we finally present the results for events with magnitude $M_w \geq 5.0$. Because of the corrections that have to be applied to the raw data, we found that there was insufficient data to examine temporal correlations for magnitude thresholds much greater than this. We also report for the first time an artefact of the directional distribution due to the poor hypocentral depth resolution of a large fraction of the data in the CMT catalogue. Once these events are removed our main conclusions are that long-range triggering in a statistical sense is detectable up to a distance of 150 km, with typical correlation lengths of 20 km or so, and that there is no strong directional dependence with respect to the orientation of the focal mechanism of the main shock.

2. Principle of the Detection of Triggering Effects in Global Seismicity

[6] To determine the distance over which triggering effects are effective in global seismicity we use the centroid moment tensor (CMT) catalogue provided by Harvard University. The data available at the time of the study are the 17,329 earthquakes that occurred between 1 January 1977 and 30 September 2000. We are interested in triggering detection, so we regard each earthquake as a

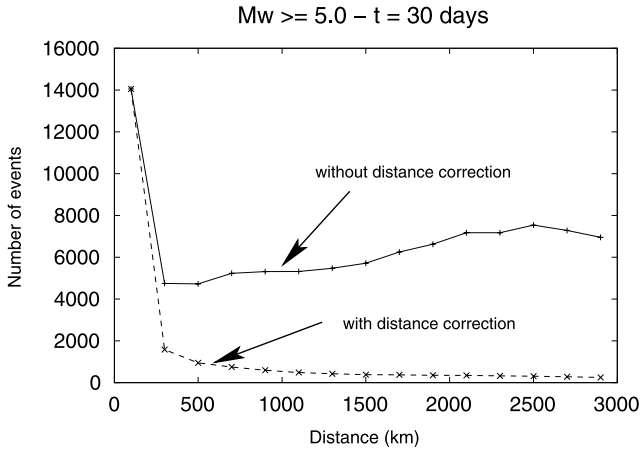

Figure 1. Plot of the number of events following a potential triggering event as a function of distance for earthquakes of magnitude larger than or equal to 5.0 during 30 days of observation. After an initial decrease, the probability of having an event seems to increase at large distances because the surface area taken into account increases too. Once this is corrected (dashed line), the probability decreases continuously with distance.

possible triggering event and all the earthquakes that follow as possible triggered ones, and impose no a priori knowledge of the distance and the duration of these effects. We are also interested in any potential variation of these triggering effects as a function of the magnitude thresholds involved, so the analysis has the following elements: (1) selection of each "source" (triggering) event belonging to a given magnitude range; (2) selection of each "triggered" event belonging to a given magnitude range (which can be the same or different from the range of magnitudes chosen for the source events) that occur within a certain number of days after the source event; and (3) calculation of the distances between each source-triggered pair of events.

[7] Histograms of distances are then made from these results. However, the interpretation of these "raw" histograms in terms of distance interaction is not straightforward for two reasons: (1) the involved surface area within an annulus $d\Delta$ and hence the probability of occurrence of an earthquake increases with epicentral distance Δ and (2) the seismicity is not spatially uniform on Earth but is instead localized in active zones.

[8] A standard Euclidian correction of the distance/surface effect may be used to normalize the data [*Lomnitz*, 1995], and is illustrated in Figure 1. To suppress the spatial seismicity distribution effect, we compare the results with those obtained by applying the same procedure to "reshuffled" catalogues. These catalogues are obtained by changing randomly the order of occurrence of the earthquakes, so that the spatial seismicity distribution is kept while the possible direct triggering of one event by another is suppressed. The physical interaction effects are then observed for the ranges of distances where the results are significantly different from those obtained by averaging the results from several reshuffled catalogues, which leads to a significant reduction of the initial apparent interaction distance, as shown in Figure 2a. The average reshuffled data then comprise the "noise" against which the triggering "signal" can be measured. As the backgrounds values are relatively small compared with the values observed at short distances, the histograms may be made with bins increasing with distance (logarithmic bins in Figure 2b) in order to check if a small signal at intermediate distance is not hidden by the strong signal observed at short distances. From Figure 2b, it appears clearly that it is not the case. As these histograms are made for a given time window following each "source" event, it is possible to study the evolution with time of the triggering effects by changing the duration of this time window. The duration of the interaction is then

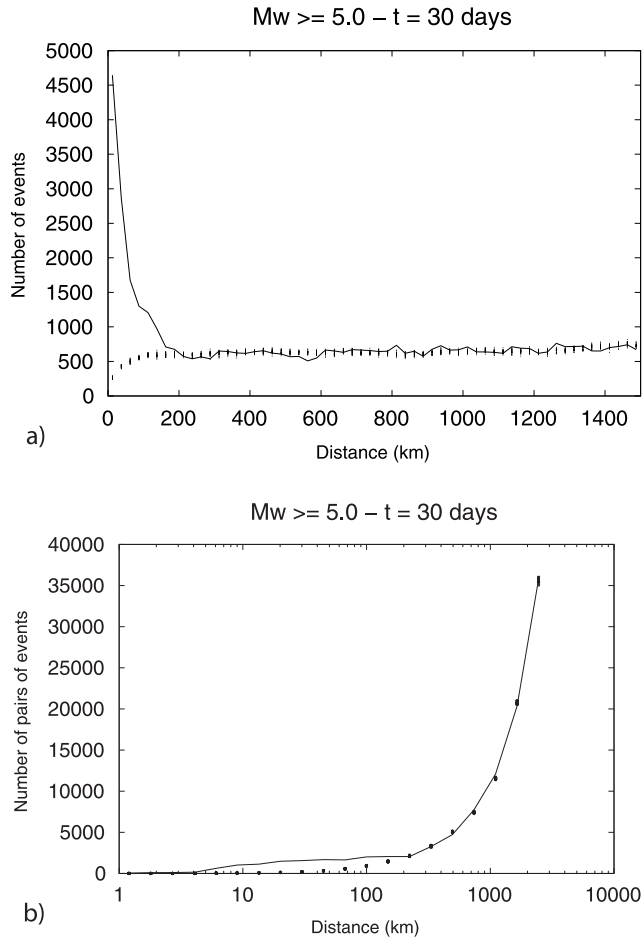

Figure 2. (a) Examples of the seismicity distribution effect. The straight lines represent the observed number of pairs of events observed for a 30 day time window without distance correction. The dots represent the results obtained by applying the same analysis to 30 reshuffled catalogues (where the order of occurrence of the earthquakes are changed). The histogram is made for 1500 km total distance and 25 km width ranges. It appears that no triggering effect is detected for distances larger than 200 km in this example. (b) Same as Figure 2a, presented with logarithmic bins. The triggering effect is not detected at longer distances than in Figure 2a.

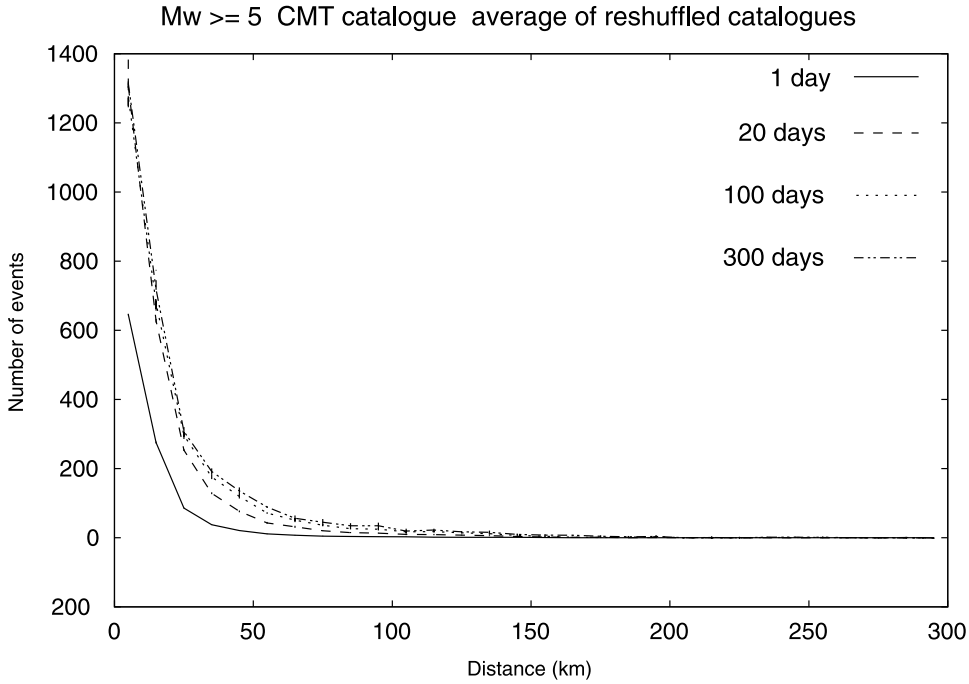

Figure 3. Examples of evolution with time of the histograms. Number of pairs of events observed for $M_w \geq 5.0$ during 1, 20, 100, and 300 days after each triggering event. Here, the distance effect (Figure 1) and the seismicity distribution effect (Figure 2) are removed. The cumulative triggering effect no longer increases between 100 and 300 days.

the time after which the increase in real seismicity is no longer significantly different from the increase in background seismicity, obtained with the reshuffled catalogues. Our null hypothesis is then a Poisson process in time, but which is localised in space due to tectonic forces and preexisting structures. From Figure 2, this null hypothesis cannot be rejected when the triggering distance is greater than 200 km.

3. Evolution of the Interaction With Time

3.1. Magnitudes $M_w > 5.0$

[9] We first study the triggering effect for all the earthquakes of magnitudes M_w larger than or equal to 5.0 and of depth less than 100 km, which represents 13,798 events. Figure 3 shows the evolution with time of the number of pairs of events separated by a distance less than 300 km. The results are presented as histograms (in 10-km-wide increments) for four durations (1, 20, 100, and 300 days). The spatial seismicity distribution effect has been removed in this diagram by substracting the histogram obtained by averaging those obtained for five reshuffled catalogues. The vertical bars represent the effect of statistical variability in the synthetic catalogues indicated by the scatter of points for the synthetic catalogues in Figure 2. It can be observed clearly on Figure 3 that (1) the cumulative triggering effect increases continuously between 1, 20, and 100 days but has effectively stabilized between 100 and 300 days, and (2) the triggering has stopped clearly before 200 km, more likely between 100 and 150 km. There is no "intermediate zone" where seismicity is reduced, compared to a Poisson process (as suggested by *Lomnitz* [1996] on the basis of statistics on a very few large events). Other histograms including larger distances have been made in order to check the possible existence of a long-range triggering effect. As none of them has shown such a feature, the histograms presented after this point are limited to a triggering distance of less than 300 km.

[10] To quantify the evolution of the triggering effect with time, the histograms are then fitted by the simple correlation relation:

$$p(r) = Ar^{-\alpha}e^{-r/L}, \tag{1}$$

where $p(r)$ is the probability density of triggering at a distance $r \pm dr/2$, A, α and L are model parameters, L being the correlation length. Equation (1) applies both to statistically based percolation models [*Stauffer and Aharony*, 1994] and to physical models for critical point phenomena [*Yeomans*, 1992]. The latter concept provides a good explanation for the general scaling properties of earthquakes [*Turcotte*, 1992; *Main*, 1996]. Moreover, the use of a distribution with power law (long-tailed) and exponential (characteristic length) components allows the relative importance of these two distribution types to be determined by the data.

[11] Figure 4 shows the results of curve fits to the incremental probability $P(r) = p(r)\,dr$, where $p(r)$ is given by equation (1) for three durations already shown (1, 20, and 100 days) for dr = 5 km. For each of them, the fit is very close to the data as indicated by the very small χ^2 (Table 1). It can also be noticed in Figure 4 and in Table 1 that L increases continuously with the time since the triggering event, but only very slightly (from 13.3 km for 1 day to 18.8 km for 300 days). The power law exponent is also

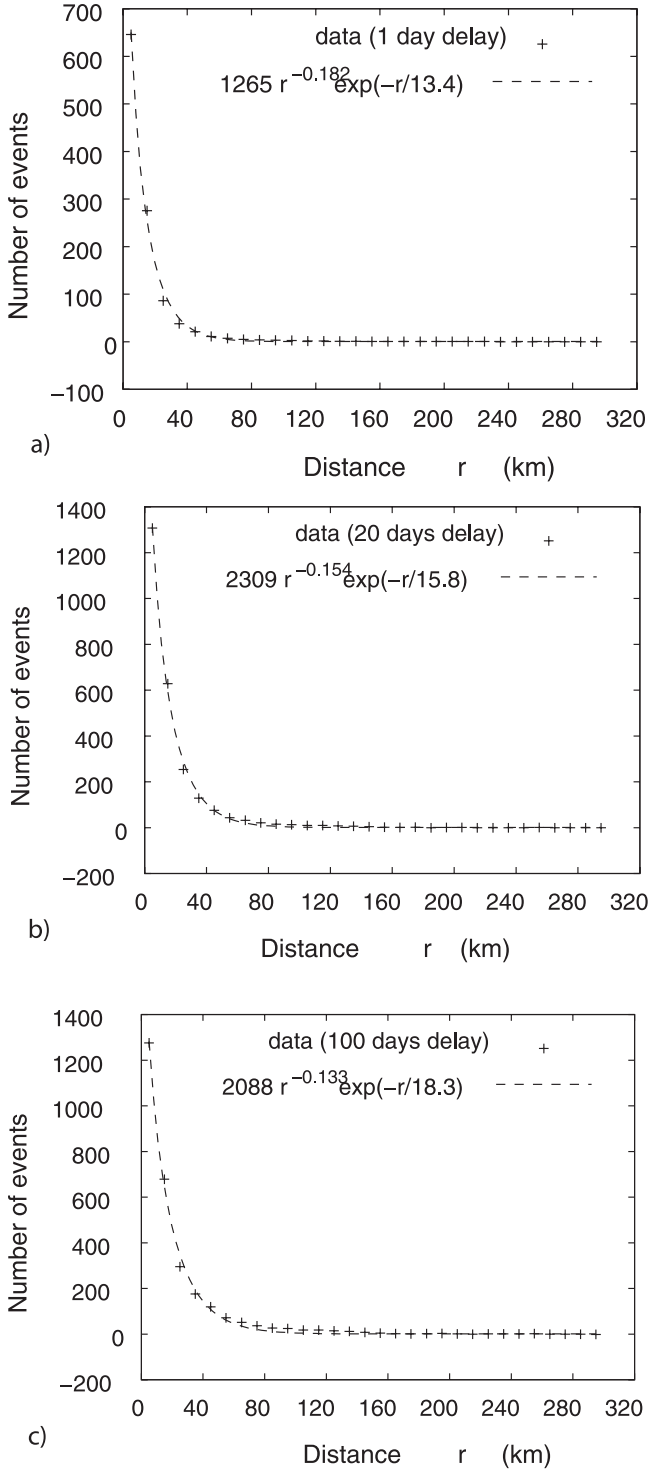

Figure 4. Fitting of the histograms by the relation $P(r) = Ar^{-\alpha}e^{-r/L}$. The crosses indicate the results while the dotted lines indicate the fits. (a) 1 day; (b) 20 days; (c) 100 days.

relatively constant, at around 0.15 ± 0.03, although it decreases systematically with time. Its low value implies that the exponential component dominates, except for very short distances.

[12] Figure 5 shows the evolution with time of the correlation length L, the mean trigerring distance, $\langle r \rangle$, α and A. The mean triggering distance is the first moment of its probability distribution

$$\langle r \rangle = \frac{\int_0^\infty p(r) r dr}{\int_0^\infty p(r) dr} = \frac{\int_0^\infty r^{-\alpha+1} e^{-r/L} dr}{\int_0^\infty r^{-\alpha} e^{-r/L} dr}. \quad (2)$$

After a change of variables to $u = r/L$, and noting that $\Gamma(a+1) = \int_0^\infty e^{-u} u^a du = a\Gamma(a)$ where Γ is the gamma function,

$$\langle r \rangle = (1-\alpha)L. \quad (3)$$

The prediction is consistent with the data shown in Figure 5a for $\alpha \approx 0.15$. For $\alpha = 0$ (a purely exponential relationship), the mean triggering distance would equal the correlation length L and the two curves on Figure 5a would overlap. Both $\langle r \rangle$ and L increase continuously with the duration involved, but at a very small rate. The slopes H of the fitting curves for $\langle r \rangle$ and L (on a double-logarithmic plot) are both close to 0.06 which is very small compared with the value of 0.5 that would be expected for a normal diffusion mechanism with $\langle r \rangle \sim t^{1/2}$. This suggests that stress diffusion for large events is "anomalously" slow. Figures 5b and 5c show the evolution with time of α and A, respectively, defined in equation (1). It can be seen from Figures 5a and 5b that $L(t)$ and $\alpha(t)$ follow power laws:

$$L(t) = a_1 t^{H_1} \quad (4)$$

$$\alpha(t) = a_2 t^{H_2}, \quad (5)$$

while $A(t)$ can be fitted by

$$A(t) = A_0 \int_0^t x^{-q} \exp(-x/T) dx \quad (6)$$

where x is a dummy variable. We see on Figure 5c that $A(t)$ has the form of an incomplete gamma function. Its density function is similar to Omori's law for aftershocks, truncated for largest times to account for the stabilization in triggering frequency shown on Figure 3 at long timescales. The

Table 1. Results of the Fitting With $Ar^{-\alpha}e^{-r/L}$ for Magnitudes $M_w \geq 5.0$

Numbers of Days	L, km	α	A	χ^2
1	13.3	0.18	1265	0.003
2	14.1	0.17	1426	0.003
3	14.6	0.17	1533	0.003
5	15.1	0.16	1688	0.003
7	15.5	0.16	1791	0.003
10	15.8	0.16	1915	0.003
20	15.8	0.15	2305	0.002
30	16.0	0.15	2568	0.002
60	15.3	0.16	2677	0.002
100	18.2	0.13	2488	0.004
180	18.3	0.13	2461	0.004
300	18.8	0.13	2320	0.006

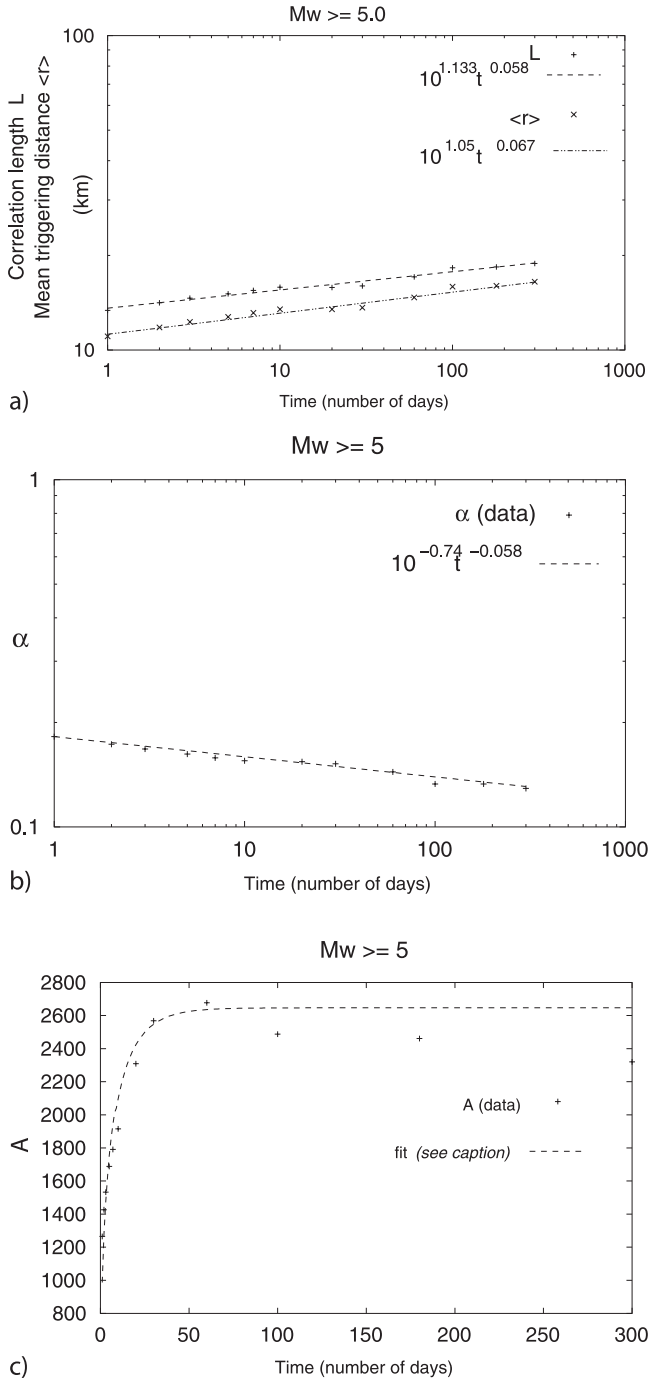

Figure 5. Evolutions of the fit parameters (equation (1)) with the duration for the events with $M_w \geq 5.0$. (a) Correlation length L and mean distance $\langle r \rangle$ (defined by equation (2)). The data (crosses) are fitted by straight lines with very small slopes (0.058 for L and 0.067 for $\langle r \rangle$). (b) For $\alpha(t)$, the data (logscale) are fitted by a straight line. (c) For $A(t)$, fitted with $A(t) = A_0 \int_0^t x^{-q} exp(-x/T)\, dx$, with $A_0 = 406$, $T = 15$, and $q = 0.60$.

conditional probability $P(r, t)$ of occurrence of an earthquake occurring at an epicentral distance $r \pm 5$ km, within a time period t since the triggering event for magnitudes $M_w \geq 5.0$, is then given by combining equations (1), (4), (5), and (6), with the following parameters: $a_1 = 13.6$, $H_1 = 0.06$, $a_2 = 0.18$, $H_2 = -0.06$, $q = 0.60$, $T = 16$ days, $A_0 = 406$ events, or a probability in equation (1) of 406/13798 = 0.029. This corresponds to an amplitude of 3% for this effect on a global scale. The data on which these are based are given in Table 1. This provides a quantitative model for the conditional probability of triggering that could be used in calculations of time-dependent seismic hazard.

3.2. Other Ranges of Magnitudes

[13] We now perform the same analysis for all the earthquakes of magnitudes M_w larger than or equal to 5.5 and of magnitudes larger than or equal to 6.0 which represents respectively 6715 and 2190 events (to be compared with the 13,798 events analyzed above with $M_w \geq 5.0$). As above, the "triggering" and the "triggered" threshold magnitudes are first set equal. Figure 6 represents the final results in terms of mean triggering distance $\langle r \rangle$ (equation (2)) as a function of time. The mean triggering distance for $M_w \geq 5.5$ is no greater than that observed for $M_w \geq 5.0$, while the mean distance for $M_w \geq 6.0$ is slightly smaller than for the two other ranges. However, the latter results may be an artefact of the paucity of available data, which leads to larger uncertainties in the parameters. Nevertheless, the rate constants for evolution with time do not seem to differ significantly with threshold magnitude. Last, we show on Figure 6 the evolution with time in cases where the threshold chosen for the source (triggering) and triggered events may differ. Here the possible triggered events are of magnitude larger than 5.0, as in the initial study (section 3.1), but the source events are larger ones ($M_w \geq 5.5$, $M_w \geq 6.0$, and $M_w \geq 6.5$). It can be seen on Figure 6 that the mean triggering distance increases slightly, this time, with the triggering event magnitude threshold.

[14] These various evolutions may be interpreted as the results of the competing effects between the energy released and consequent stress redistribution amplitude (which depends on the magnitude) and the average distance between possible events of a given magnitude, which itself depends to first order on the preexisting stress state of the lithosphere, which may have strong rheological and structural controls, for example the seismogenic thickness. We might expect a difference of 0.5 in triggering magnitude to

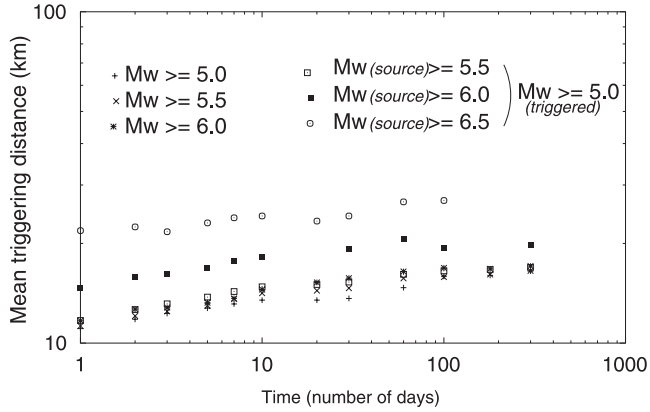

Figure 6. Evolution of the mean distance $\langle r \rangle$ with the duration (logscale) for various ranges of magnitudes thresholds (both for source and triggered events).

imply a larger triggering distance. However, the average distance between possible events larger than a certain threshold, also increases with this magnitude threshold. The systematic negative correlation of rupture size and separation of fault tips between similarly sized events may explain why the triggering distance of similarly sized events is only weakly magnitude dependent, while the triggering mean distance, when the triggering threshold is the larger seems, on the contrary, magnitude-dependent. In any case, the magnitude dependence to first order is weak, implying that the preexisting stress heterogeneity, coupled to a strong rate-dependent ''clock-advance'', may be the strongest control on the observations.

4. Normal Stress Effects

4.1. Introduction

[15] If the normal stress change affects triggering, then the orientation of the triggered event with respect to the orientation of the focal mechanism should show some directional dependence [*Kagan and Jackson*, 1998]. For example, by analyzing global catalogues, *Lomnitz* [1996] suggests that, for the largest events this century, global seismicity is increased in the dilatation zones while reduced in the compression zones compared to a Poisson process. In this section, we aim to determine whether or not the sign of the normal stress change (compression or dilatation) induces systematic differences in stress triggering at the global seismicity scale.

4.2. Method

[16] The data used here are taken from the CMT catalogue which also gives the two nodal planes for each focal mechanism. For each pair of ''source''-''triggered'' events (which will be referred as S and T events) we use the focal mechanism of the S event and examine in which type of quadrant (compression C or dilatation D) the T event is located. The focal mechanism is expressed in terms of strike Φ, dip δ and rake λ for the two nodal planes following the common convention described by *Aki and Richards* [1980, Figure 4.13].

[17] If the fault plane and the slip vectors are known, a simple geometrical analysis allows us to determine in which type of quadrant the T event is located. First, the difference between the direction of the T event (azimuth Az) and the fault direction (strike Φ) (Figure 7a) and the difference of depths between the S and T events (associated with the knowledge of the fault dip) (Figure 7b), indicates if the T event belongs to the hanging wall or to the footwall. Then, the sign of the scalar product between the slip vector **u** and the direction **ST** associated with the knowledge of the type of wall indicates the type of quadrant: for the T event in the hanging wall, $\mathbf{u} \cdot \mathbf{ST} > \mathbf{0}$ indicates a compression quadrant while $\mathbf{u} \cdot \mathbf{ST} < \mathbf{0}$ indicates a dilatation quadrant. The opposite results are obtained for the footwall. From the above, we examine only the effect within 200 km, which simplifies the calculations significantly.

[18] From the definition of the nodal planes, the analysis previously described should give the same results for both the real fault plane and the auxiliary nodal plane. As an internal consistency check, we carried out the analysis for both planes in order to estimate potential errors due to the precision of the calculations. Results show that less than 1% of the results differ when changing from one plane to another. This always occurs when the triggered event is localized very near to either nodal plane, that is when it is neither clearly in compression nor in dilatation. These few uncertain results are then removed for following the analysis.

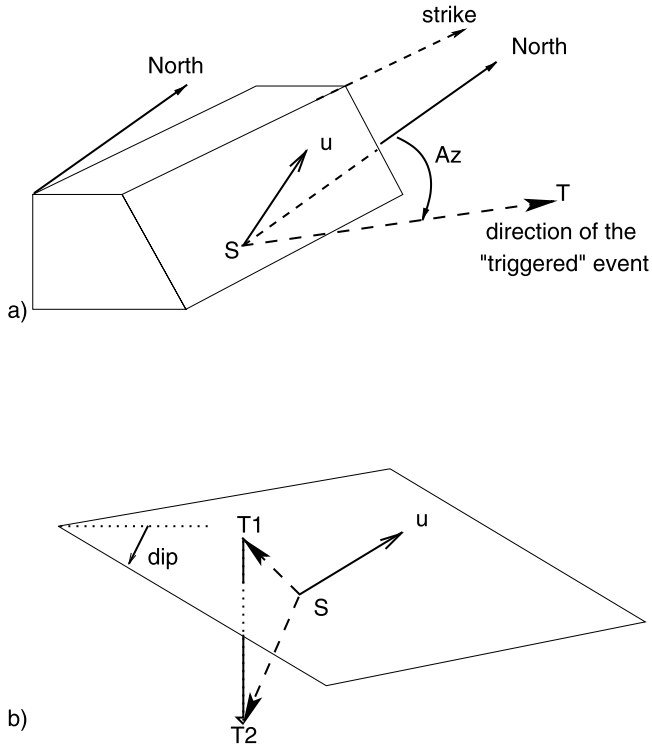

Figure 7. Determination of the direction and the wall (i.e., footwall or hanging wall) in which the triggered event T is located. The determination takes into account both: (a) the azimuth Az of the triggered event, compared with the fault direction (strike Φ) and (b) the difference of depth between source and triggered event. For a same difference $Az-\Phi$ the depth (triggered event T_1 or T_2) changes the wall.

4.3. Differences Observed Between Compression and Dilatation Quadrants

[19] The analysis explained in section 4.2 is now applied to the same data as before (magnitude $M_w > 5.0$) in order to examine the extent of directional preferences in triggering with respect to source orientation. Figure 8a shows the numbers of earthquakes observed in dilatation and compression quadrants for a duration of 30 days. Since dividing the data set in two parts (N/2) reinforces the noise effect, a large time windows has to be chosen in order to use as many data as possible. It appears at first sight clearly on Figure 8a that more events occur in the dilatation quadrants than in the compression ones. The histograms are not corrected at this stage for the distance effect in order to make easier a rough graphical determination of the maximum distance for which the differences between quadrants seem significant. Figure 8b shows the ratio of numbers of events in dilatation/compression (D/C) quadrants for 30 days delay. D/C is larger than 1.0 until approximately 160 km

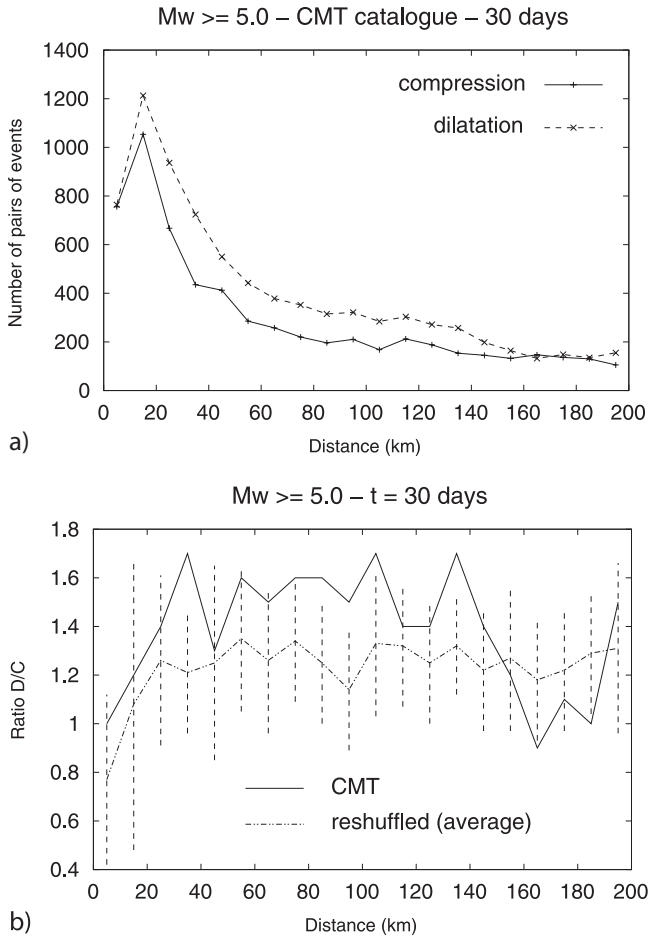

Figure 8. (a) Number of events within a distance $r \pm \delta r$ ($\delta r = 5$ km), for the two quadrants of the source events focal mechanism. (b) Ratio of events D/C calculated from Figure 8a. The data (solid lines) are compared to synthetic results from a range of synthetic catalogues (dashed lines) within the range of variability (vertical dashed lines). Even the random synthetic catalogues show a preference for the dilational quadrant, except at very short distances.

(from its smallest value 1.0 for the shortest distance up to 1.7 at 35 km, 105 km, and 135 km with an average value equal to 1.39). However, on the same figure, the histograms made with several reshuffled catalogues also show a preference for the dilatation quadrant, despite the absence of a triggering signal. This implies that at least a component of the preference for the dilational quadrants is purely due to the spatial distribution of event pairs relative to their focal mechanism.

[20] In summary, the directional effects determined from an uncritical application of the CMT catalogue data do appear to show a small systematic triggering preference for the dilatational quadrant but a significant portion of this is likely to be a spatial correlation effect. In section 4.4, we examine the effect of uncertainties in depth on the directional dependence of earthquake triggering for events with a significant dip-slip component. To understand this effect, we first have to note more precisely the distribution of focal mechanisms. Figure 9 shows the distribution of rakes found in the CMT catalogue for both nodal planes. The fact that the catalogue is dominated by faults with a significant oblique rake (i.e., predominantly reverse, but also normal faults) introduces a further potential artefact in the analysis which we address in section 4.4.

4.4. Depth Effect

[21] The depth of the earthquakes, often rather uncertain, is a critical parameter for the determination of the azimuth between source and receiver, and hence on the quadrant, as shown in Figure 7b. As a consequence, any systematic uncertainty in the depth determination may propagate into a systematic change in the azimuth of the triggered event and, hence, a change of the quadrant.

[22] The depth distribution of the CMT catalogue events shows two very large peaks that appear at the starting depths of the source inversion, with 2874 and 5521 events at respectively 10 km and 33 km, while the background values around these depths rarely exceed 100 per 1-km-wide counting increment. Such events essentially have undetermined depths. This problem in the depth determination is an important one in our study (events of depth less than 100 km) because our calculation of the orientation relative to the focal sphere depends critically on the relative depths of the source and triggered events. To see the possible effect of this poor depth determination on the results, we repeat the previous analysis on a catalogue ($M_w \geq 5.0$) where all the events located at the starting depths of the hypocentre inversion at 10 km (that is 2810 events) and 33 km (5413 events) are removed. We then use a reduced catalogue of only 5575 events instead of 13,798 events. This large reduction illustrates how the depth is usually the least well constrained parameter in the earthquake source. The results, for comparison with Figure 8a ($M_w \geq 5.0$), are shown on Figure 10. As expected, they are slightly more noisy because fewer pairs of events are involved. Moreover, the difference between compression and dilatation does not appear as clear as for the whole set of events. There are now more events in the compression quadrants than in the dilatation ones in the first 20 km. After this distance, slightly more events are located in the dilatation zones. However, a more precise analysis of the ratio dilatation/compression for

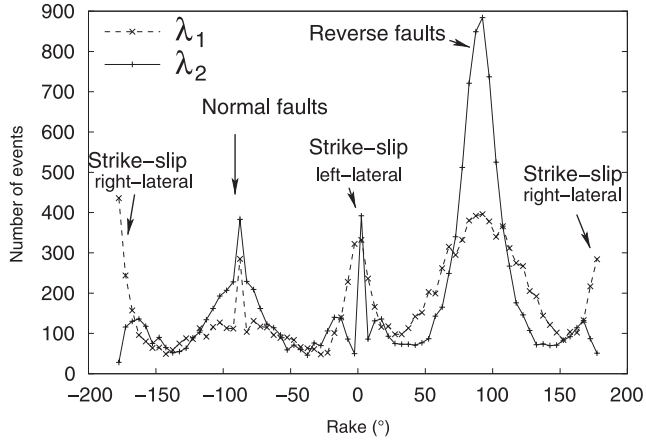

Figure 9. Distribution of the faults rakes (CMT catalogue) with respect to the two nodal planes (5° increments).

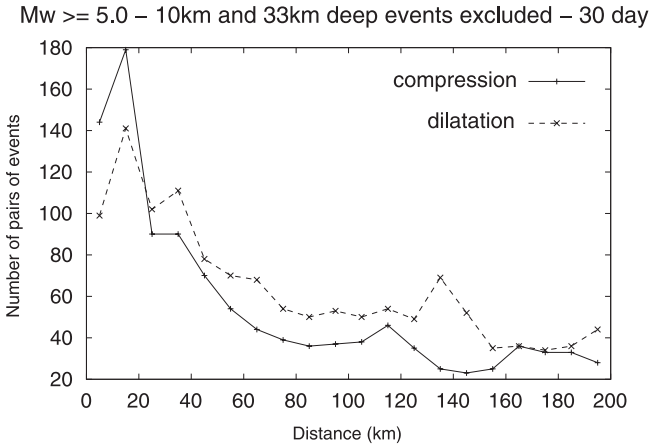

Figure 10. Same as Figure 8a except that all the events located either at 10.0 km or 33.0 km depth are removed from the data.

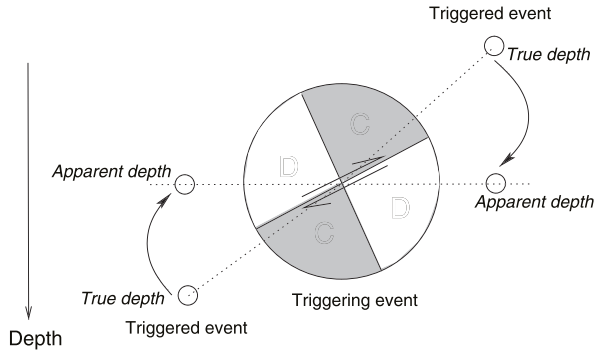

Figure 12. Geometrical explanation of the artefact introduced by the systematical localization of the events at a constant depth-pure reverse fault case. If triggered events are forced to be at the same depth than the triggering event, they are forced to be in the dilatation zones.

a set of synthetic catalogues shows that the differences between compression and dilatation are of about the same amplitude as the variations observed for the CMT data. We conclude that the apparent trend observed in Figure 8a does not appear to be statistically significant for events with well-determined depths in the CMT catalogue in Figure 10.

[23] To understand more thoroughly the role played by the events for which depth remains unknown (33 and 10 km), the same analysis for the events located at 33 km (predominantly subduction zone events) is shown on Figure 11. Figure 11 shows a apparently clear preference for the dilatation until 160 km. However, the same analysis applied to reshuffled data indicates the same difference in favor of the dilatation quadrant. Hence the data, removed of potential artefacts, show no clear directional dependence for the triggering frequency. Why might the depth artefact lead to an enhanced preference for the dilational quadrant in addition to the random effect caused by the spatial distribution of earthquakes relative to their focal mechanisms as shown if Figure 8b? Figure 12 illustrates a potential example for the pure reverse fault case. If two reverse faulting events with shallow dip but different actual depths are forced to have exactly the same depth, then the triggered event is also forced to be geometrically in the dilatation zone. The opposite feature would be observed for the normal faults. This geometrical effect is of course only valid for pure reverse or pure normal faults. In contrast, for a strike-slip fault with a 90° dip, the depth determination has no influence on the azimuth, and hence on the compression/dilatation quadrant. These cases are obviously extreme ones, and for a mixed mechanism (reverse/strike-slip or normal/strike-slip) the probability depends on the relative importance of each mechanism. However, the distribution of the focal mechanisms for the events located at 33.0 km show a clear preference for the reverse fault mechanism as shown on the histograms of rakes (Figure 13). The probability of having an event in a dilatation zone will therefore be higher than that to have it in a compression zone, simply because of the predominance of reverse mechanism, enhanced by the depth artefact. The opposite feature may be observed for the normal faulting events typically located at 10 km depth, but with a much smaller

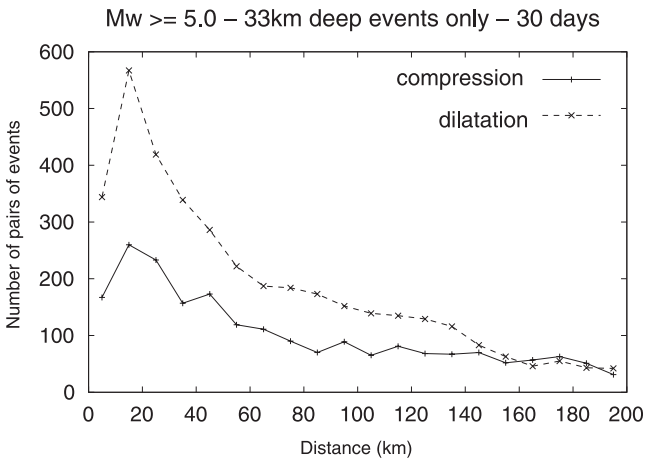

Figure 11. Same as Figure 8a for events located at 33.0 km only.

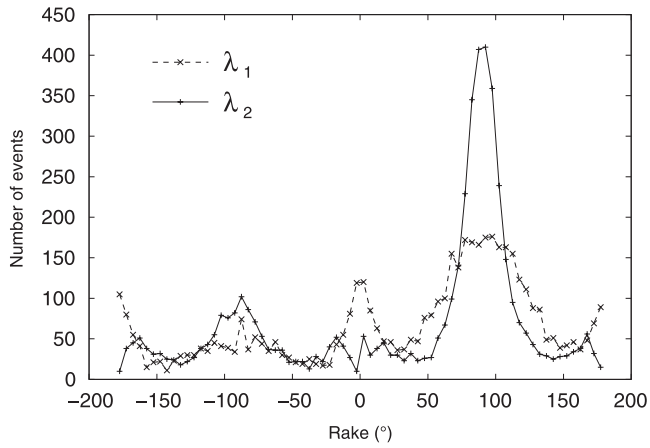

Figure 13. Histograms of the rakes of the earthquakes located at 33.0 km depth.

amplitude, because of a smaller number of events. We conclude that a significant component of the apparent directionality in triggering-triggered events pairs is due the spatial distribution of event type, exacerbated by an artefact of poor depth determination. When this is accounted for, we see no statistically significant preference for the compressional or dilational quadrants, and hence no strong normal stress effect, consistent with *Kagan and Jackson*'s [1998] results.

5. Discussion

[24] Our results have shown several interesting, and some unexpected features. First, we clearly observe a long-range triggering effect in global data which has been corrected for the known artefacts, including a subtle effect due to the distribution of focal mechanisms and uncertainty in seismic depth not previously noted. This implies that it is not easy to compare our results directly with previous studies, and that certainly these effects should be taken into account in future work.

[25] We find that the histogram of triggered events as a function of distance can be fitted very well by a power law in the near field, with an exponential tail in the far field. Such correlation distributions are also found in critical point phenomena [*Yeomans*, 1992] and near the percolation threshold [*Stauffer and Aharony*, 1994]. This might suggest that at least one of the reasons earthquakes may be relatively easy to trigger is that the crust at a global scale is already in a near-critical state [*Bak and Tang*, 1989; *Main*, 1996]. It is also consistent with the notion of clock advance for events [*Gomberg et al.*, 1997] that were at least near failure prior to the main shock as a consequence of the rate and state dependence of the frictional constitutive law discussed in the introduction. The low value of the power law exponent in equation (1) implies that the spatial correlation can be fitted to a good first approximation by an exponential. In all cases a triggering signal can be seen above the background 'noise' up to a distance of 150 km or so, i.e., of the same order of magnitude as the lithospheric thickness. This result is in good agreement with the regional study of Italian earthquakes by *Gasperini and Mulargia* [1989]. The correlation length L from the exponential component is of the order 20 km, i.e., of the same order of magnitude of the thickness of the seismogenic zone.

[26] There is no strong dependence of L on the triggering magnitude, and hence on the magnitude of the local static or dynamic stress change. This suggests that the range within which triggered events may occur has some strong a priori structural constraints, e.g. the thickness of the seismogenic crust, or the thickness of the lithosphere discussed above, and depends only weakly on the size of the triggering event, or the magnitude of the change in static stress. This is also consistent with the weak directional dependence of the triggered event with respect to the orientation of the focal mechanism of the source event.

[27] We observe that both L and the mean triggering distance increase systematically with time according to a power law t^H with a very small exponent ($H = 0.06$), certainly much less than $t^{1/2}$ dependence expected from an homogeneous diffusion process. Similar low values of H have been reported for mining-induced seismicity by *Marsan et al.* [1999, 2000]. This might imply that stress diffusion is inhomogeneous on a large range of scales, more akin to "anomalous diffusion", in materials where transport of some property is channelled. For example, the dispersion of tracers in fluids at low Raleigh number in homogeneous porous media is well fitted by a homogeneous diffusion law. In contrast, tracer dispersion in fracture networks is "anomalous" in several senses [*Berkowitz and Scher*, 1998]. First, the concentration profile is not a symmetric Gaussian, but instead takes the form of a skewed distribution, with a few particles at greater distances, but more "held back" near the source. This results in slower diffusion of the average length, with the time-dependent exhibiting an exponent smaller than 1/2. This is consistent with our observation of a low exponent, with most of the effect confined near the source (<20 km), but with a longer range of influence than might be expected from average properties (<150 km). This characteristic behavior was first derived for anomalous transport in semiconductors, but has also been applied to pollutant transport. The main physical theory for the occurrence of anomalous transport is the Continuous Time Random Walk, which generalizes the standard Random Walk theory for homogeneous diffusion in two main senses [*Berkowitz and Scher*, 1998]. First, the time step between individual steps can occur at any time, not just at discrete and equal time intervals and, second, that the step length is not constant, but sampled from a power law distribution. In this sense the transport properties are akin to a Lévy flight [*Sotolongo-Costa et al.*, 2000].

[28] In any event, we conclude that stress diffusion by triggering is definitely not homogeneous, but instead shows all the hallmarks of "anomalous" diffusion. Therefore stress triggering cannot be modelled with a simple rheology involving homogeneous stress diffusion with a $t^{1/2}$ time dependence. In physical terms, this implies that, for the problem of earthquake triggering, we cannot ignore the spatial heterogeneity of the preexisting structures and stress field at scales below the correlation length. This implies that an appropriate elemental volume above which the crust can be assumed to be spatially uniform for the problem of stress diffusion is similar to the dimensions of the brittle crust (10–20 km).

[29] In the problem of transport during fluid flow, there is a clear physical mechanism for non-Gaussian diffusion in the form of channelling in a medium of heterogeneous permeability. What might be the underlying physical cause for such behavior in the problem of stress diffusion by triggering? One possible cause might be the time dependence introduced by the rate- and state-dependent friction theory [*Dieterich*, 1994]. This model was applied by *Marsan et al.* [2000, Figure 14] to the problem of anomalous diffusion during triggering for a preexisting system of faults with a fractal dimension D. They found that the constitutive laws from rate-dependent friction do predict the functional form of the stress diffusion very well, but the power law form was only recovered with an exponent $H \simeq 0.3$ for reasonable values of the model parameters, notably the ratio of stress drop to ambient stress. This value for H is much higher than that reported here or by *Marsan et al.* [1999, 2000].

[30] If frictional theory cannot account quantitatively for the observed spatiotemporal evolution for the triggering

phenomenon, then what alternatives might there be? One possibility might be due to the acceleration of time-dependent subcritical crack growth by stress corrosion [*Das and Scholz*, 1981; *Main*, 1988]. This theory uses the experimental observation that the velocity of crack growth depends nonlinearly on the stress intensity

$$K = Y\sigma c^{1/2} \tag{7}$$

where σ is the remotely applied stress, c is the fracture semilength, and Y is a dimensionless geometrical constant that depends on the loading geometry and the failure mode (tensile, in-plane or antiplane shear). Experimentally, the form of the nonlinearity is

$$\frac{dc}{dt} = V_0\left(\frac{K}{K_0}\right)^n \tag{8}$$

where V_0 is a reference initial velocity at time t_0, and K_0 is the initial stress intensity. The stress perturbation of a crack in an infinite medium at a distance r and angle θ from the crack tip is

$$d\sigma = K(2\pi r)^{-1/2} f_{i,j}(\theta) + X \tag{9}$$

where f describes the azimuthal variation with respect to the crack orientation and X is a constant [e.g., *Atkinson and Meredith*, 1987]. We imagine there is a preexisting fault that is growing subcritically at position and distance (r, θ) from the triggering event. From equations (7) and (8) we can write the triggering effect at this position in terms of a perturbation in the stress $d\sigma(r, \theta)$

$$\frac{dc}{dt} = V_0\left(\frac{\sigma_0 + d\sigma}{\sigma_0}\right)^n \left(\frac{c}{c_0}\right)^{n/2} \tag{10}$$

If we neglect the directional effect in equation (9), we have

$$d\sigma = d\sigma_{r_0}\left(\frac{r}{r_0}\right)^{-1/2} \tag{11}$$

where r_0 is a reference distance that might for example be the dimensions of the process zone of damage ahead of the crack tip. If the process zone is small compared to the triggering distance r, i.e., $r \gg r_0$, then from equations (10) and (11),

$$\frac{dc}{dt} = V_0\left(\frac{d\sigma_{r_0}}{\sigma_0}\right)^n \left(\frac{r}{r_0}\right)^{-n/2} \left(\frac{c}{c_0}\right)^{n/2} \tag{12}$$

The solution of this differential equation with limits $t_0 = 0$ and time t, for $n > 2$, is

$$c = c_0\left[1 - t/t_f\right]^{-\nu} \tag{13}$$

where

$$\nu = \frac{2}{n-2} > 0 \tag{14}$$

and the failure time t_f is

$$t_f = \frac{\left(\frac{2}{n-2}\right)c_0}{V_0\left(\frac{d\sigma_{r_0}}{\sigma_0}\right)^n \left(\frac{r}{r_0}\right)^{-n/2}} \tag{15}$$

If the failure time at (r, θ) specifies the origin time and location of the triggered event, then we have from equation (15) a relation of the form

$$r(t) \propto t^{2/n} \tag{16}$$

That is, we recover the same anomalous diffusion profile as the rate-state theory, but with $H = 2/n$, rather than $H = 0.3$. Typical empirical values of n for crystalline rock from laboratory experiments are $n = 30$ for basalt [*Atkinson and Meredith*, 1987] and $n = 24$ for an earthquake nucleation event reported by *Das and Scholz* [1981]. Here we find $H_o \simeq 0.06$, implying $n \simeq 33$, i.e., very similar to the observational range. We note from equation (15) that the constant of proportionality in equation (16) would also depend on the ratio of stress drop to ambient stress. However, unlike the rate and state theory of *Dieterich* [1994] applied by *Marsan et al.* [2000], it does not affect the magnitude to the exponent H. This might explain why the values of the exponents calculated in this paper are relatively insensitive to the triggering threshold magnitude, and why there appears to be no lower threshold to the problem of stress transfer and earthquake triggering in general [*Ziv and Rubin*, 2000].

[31] Despite the prediction of a directional component of the triggering frequency (either due to rate-and-state friction or equation or the accelerated subcritical crack growth theories described above), we observe no strong directional dependence in the observed triggering as a consequence of the first-order static stress change represented by the main shock focal mechanism. After correction for an artefact related to the distribution of focal mechanisms and unknown source depth in the CMT catalogue, we find that earthquakes are equally likely to be triggered in both compressional and dilational quadrants of the main shock focal mechanism. This is in direct contrast to the strong directional dependence of aftershock sequences, particularly with Coulomb stress changes [e.g., *Stein et al.*, 1992]. *Kagan and Jackson* [1998] interpreted the lack of a strong directional effect in terms of a near-zero static friction coefficient. The weak directional dependence is also internally consistent with the derivation of equation (1), which assumes a correlation length that is independent of direction [*Yeomans*, 1992, p. 20]. A more detailed investigation of the validity of this assumption to second order awaits a solution to the fault plane/auxiliary plane ambiguity for global data sets.

[32] In the above, we have concentrated on the phenomenon of stress triggering in a brittle elastic medium with time-dependent rheology over relatively short timescales. However, a full theory would also include the effect of plastic deformation in the lithosphere. Interestingly, time-dependent calculations of stress perturbations which incorporate such a layered rheology [*Roy and Royden*, 2000, Figure 4a] do show long-lived stress perturbations which peak at a distance $r = 10$–20 km away from a major fault,

and decay to zero for $r > 150$ km or so. Quantitatively, these values correspond closely to our values for (1) the correlation length and (2) the maximum range of influence respectively, consistent with our inference that the two are conditioned strongly by the thickness of the (1) brittle crust and (2) the lithosphere. They are also much lower than the several thousand km for long-term triggering inferred by *Kagan and Jackson* [1991]. *Roy and Royden* [2000] did not calculate the stress diffusion exponent H explicitly, but the slow rates of stress diffusion they predicted are indicative of anomalous diffusion also being applicable on geological timescales, consistent with the small values of H inferred here.

6. Conclusion

[33] We have examined in detail the properties of earthquake triggering for moderate and large events in the global CMT catalogue. We find no evidence for very long range triggering at distances of several hundred km, and find that a typical range of influence is of the order less than 150 km. The separation distance between source and triggered events can be well fitted by a gamma distribution, of identical form to that observed for correlation functions in statistical physics near (but below) the critical point, with a finite correlation length. The correlation length is of the order 10–20 km, and both the correlation length and the mean triggering distance increase with time in the power law form t^H, where $H \sim 0.05–0.06$, much less than $H = 0.5$ predicted from an homogeneous stress diffusion process. After correction for an artefact of poor depth determination, we find no evidence for a directional triggering dependence, implying a stronger rate dependence in triggering than that implied by the magnitude and sign of the static normal stress change. The magnitude of the anomalous diffusion exponent H can be explained quantitatively by a clock advance of the failure time as a consequence of the effect of the stress perturbation on the local rate of subcritical crack growth. The anomalous diffusion implies a strong structural control on the field heterogeneity, with a correlation length of similar order of magnitude to the seismogenic thickness, and a weaker but detectable correlation up to a distance of the same order of the lithospheric thickness. The functional form of the time-dependent increase in frequency of the triggered events $P(r, t)$ determined here can be used directly to estimate the conditional probability of occurrence in calculations of time-dependent seismic hazard. The amplitude of this effect on a global scale is of the order of 3%.

[34] **Acknowledgments.** This work was funded initially by NERC Connect grant GR3/C0022, with matching funding from BP/Amoco, and completed during the EU fifth framework grant ENK6-CT-2000-00056. We thank Kes Heffer, Sergei Zatsepin, and Thomas Leonard for discussions during the course of the work and David Marsan for providing preprints of his work. We thank Bob Simpson, Steve Miller, Yan Kagan, and an anonymous Associate Editor for their careful and constructive reviews of earlier manuscripts.

References

Aki, K., and P. G. Richards, *Quantitative Seismology: Theory and Methods*, W. H. Freeman, New York, 1980.

Atkinson, B. K., and P. G. Meredith, The theory of subcritical crack growth with applications to minerals and rocks, in *Fracture Mechanics of Rock*, edited by B. K. Atkinson, pp. 111–166, Academic, San Diego, Calif., 1987.

Bak, P., and C. Tang, Earthquakes as a self-organized critical phenomenon, *J. Geophys. Res.*, *94*, 15,635–15,637, 1989.

Berkowitz, B., and H. Scher, Theory of anomalous transport in random fracture networks, *Phys. Rev. E*, *57*, 5858–5869, 1998.

Das, S., and C. H. Scholz, Theory of time-dependent rupture in the Earth, *J. Geophys. Res.*, *86*, 6039–6051, 1981.

Dieterich, J., A constitutive law for rate of earthquake production and its application to earthquake clustering, *J. Geophys. Res.*, *99*, 2601–2618, 1994.

Dziewonski, A. M., G. Ekstrom, and N. N. Maternovskaya, Centroid-moment tensor solutions for July–September 2000, *Phys. Earth Planet. Inter.*, *124*, 9–23, 2001.

Gasperini, P., and F. Mulargia, A statistical analysis of seismicity in Italy: The clustering properties, *Bull. Seismol. Soc. Am.*, *79*, 973–988, 1989.

Gomberg, J., M. L. Blanpied, and N. M. Beeler, Transient triggering of near and distant earthquakes, *Bull. Seismol. Soc. Am.*, *87*, 294–309, 1997.

Harris, R. A., Introduction to special section: Stress triggers, stress shadows, and implications for seismic hazard, *J. Geophys. Res.*, *103*, 24,347–24,358, 1998.

Harris, R. A., R. W. Simpson, and P. A. Reasenberg, Influence of static stress changes on earthquake locations in southern California, *Nature*, *375*, 221–224, 1995.

Hill, D. P., et al., Seismicity remotely triggered by the magnitude 7.3 Landers, California, earthquake, *Science*, *260*, 1617–1623, 1993.

Kagan, Y. Y., and D. D. Jackson, Long-term earthquake clustering, *Geophys. J. Int.*, *104*, 117–133, 1991.

Kagan, Y. Y., and D. D. Jackson, Spatial aftershock distribution: Effect of normal stress, *J. Geophys. Res.*, *103*, 24,453–24,467, 1998.

King, G. C. P., R. S. Stein, and J. Lin, Static stress changes and the triggering of earthquakes, *Bull. Seismol. Soc. Am.*, *84*, 935–953, 1994.

Linker, M. F., and J. H. Dieterich, Effect of variable normal stress on rock friction: Observations and constitutive equations, *J. Geophys. Res.*, *97*, 4923–4940, 1992.

Lomnitz, C., On the distribution of distances between random points on a sphere, *Bull. Seismol. Soc. Am.*, *85*, 951–953, 1995.

Lomnitz, C., Search of a worldwide catalog for earthquakes triggered at intermediate distances, *Bull. Seismol. Soc. Am.*, *86*, 293–298, 1996.

Main, I. G., Prediction of failure times in the Earth for a time-varying stress, *Geophys. J. Int.*, *92*, 455–464, 1988.

Main, I. G., Statistical physics, seismogenesis and seismic hazard, *Rev. Geophys.*, *34*, 433–462, 1996.

Marsan, D., C. J. Bean, S. Steacy, and J. McCloskey, Spatio-temporal analysis of stress diffusion in mining-induced seismicity, *Geophys. Res. Lett.*, *26*, 3697–3700, 1999.

Marsan, D., C. J. Bean, S. Steacy, and J. McCloskey, Observations of diffusion processes in earthquake populations and implications for the predictability of seismicity systems, *J. Geophys. Res.*, *105*, 28,081–28,094, 2000.

Reasenberg, P. A., Foreshock occurrence before large earthquakes, *J. Geophys. Res.*, *104*, 4755–4768, 1999.

Roy, R., and L. H. Royden, Crustal rheology and faulting at strike-slip plate boundaries: 1. An analytical model, *J. Geophys. Res.*, *105*, 5583–5597, 2000.

Scholz, C. H., Earthquake and friction laws, *Nature*, *391*, 37–42, 1998.

Sotolongo-Costa, A., J. C. Antoraz, A. Posodas, F. Vidal, and A. Vasquez, Levy flights and earthquakes, *Geophys. Res. Lett.*, *27*, 1965–1969, 2000.

Stauffer, D., and A. Aharony, *Introduction to Percolation Theory*, 2nd ed., Taylor and Francis, Philadelphia, Pa., 1994.

Stein, R. S., The role of stress transfer in earthquake occurrence, *Nature*, *402*, 605–609, 1999.

Stein, R. S., G. C. P. King, and J. Lin, Change in failure stress on the southern San Andreas Fault system caused by the 1992 magnitude = 7.4 Landers earthquake, *Science*, *258*, 1328–1332, 1992.

Stein, R. S., G. C. P. King, and J. Lin, Stress triggering of the 1994 $M = 6.7$ Northridge, California, earthquake by its predecessors, *Science*, *265*, 1432–1435, 1994.

Stein, R. S., A. A. Barka, and J. H. Dieterich, Progressive failure on the North Anatolian fault since 939 by earthquake stress triggering, *Geophys. J. Int.*, *128*, 594–604, 1997.

Turcotte, D. L., *Fractals and Chaos in Geology and Geophysics*, Cambridge Univ. Press, New York, 1992.

Yeomans, J. M., *Statistical Mechanics of Phase Transitions*, Oxford Sci., Oxford, U.K., 1992.

Ziv, A., and A. M. Rubin, Static stress transfer and earthquake triggering: no lower threshold in sight?, *J. Geophys. Res.*, *105*, 13,631–13,642, 2000.

M. Huc and I. G. Main, School of GeoSciences, Edinburgh University, West Mains Road, Edinburgh EH9 3JW, UK. (mhuc@nordnet.fr; Ian.Main@ed.ac.uk)